Journal of the Franklin Institute 363 (2026) 108358

Contents lists available at ScienceDirect

Journal of the Franklin Institute

journal homepage: www.elsevier.com/locate/fi

Safety guarantee via periodic discrete-time high-order control barrier function: Application to bipedal robots

Kai Zong [a], Xiaochen Xie [a,*], Zhaoji Ling [a], Jing Dai [b,c], Ka-Wai Kwok [b]

[a] School of Intelligence Science and Engineering, Harbin Institute of Technology, Shenzhen, 518055, Guangdong, China
[b] Department of Mechanical and Automation Engineering, The Chinese University of Hong Kong, Shatin, Hong Kong
[c] Multi-Scale Medical Robotics Center Ltd., Shatin, Hong Kong

ARTICLE INFO

Keywords:
Bipedal robot
Control barrier function
Model predictive control
Periodic characteristics

ABSTRACT

In this paper, the concept of periodic discrete-time high-order control barrier function (P-DHOCBF) is developed. The proposed P-DHOCBF is utilized to ensure the forward invariance of the safety set for discrete-time systems with periodic characteristics in system states of any relative degree. Focusing on the periodic forward walking problem of bipedal robots based on the variable-height inverted pendulum model, a periodic model predictive control optimization problem incorporating P-DHOCBF is formulated, and periodicity-related constraints are established. Compared to the existing discrete-time control barrier function, the proposed P-DHOCBF significantly reduces the conservatism of safety, thereby enhancing the system safety by promptly preventing unsafe occurrences. An illustrative example and simulation results based on a 12-degree-of-freedom (DOF) bipedal robot verify the effectiveness of the proposed approach.

1. Introduction

Systems with periodic characteristics have been extensively studied in both continuous-time and discrete-time domains since the 19th century [1]. The periodic characteristics of time are widely observed in both natural phenomena and engineering applications, such as cyclic variations in ecosystems, periodic vibrations and motions in electromechanical systems, and recurrent behaviors in networked systems [2]. Over the past decade, various control techniques have been developed to address stability, stabilization, and control problems in different types of systems with dynamical periodicity [3–5]. In addition, systems with periodic characteristics in their states, whether from dynamics or kinematics, have also been widely studied [6,7]. In various operating environments, periodic and aperiodic behaviors of the systems often represent different physical phenomena and thus demand different control objectives.

In modern control theory, safety is a crucial concern in control systems, requiring that the system states remain within a predefined safety set [8]. Inspired by the concept of control Lyapunov functions, control barrier functions (CBFs) were introduced to ensure system safety by enforcing forward invariance of the safety set [9]. Several formulations of CBFs have been proposed, including exponential CBFs [10], robust CBFs [11], and high-order CBFs (HOCBFs) [12]. These formulations have been applied in various fields, such as robotic grasping [13], adaptive cruise control [14], and obstacle avoidance for robots [15]. However, to the best of our knowledge, safety guarantees for periodic characteristics in system states have received little attention in the existing literature.

Model predictive control (MPC) is a well-established approach in modern control and has been widely employed in applications such as robotic motion and manipulation [16]. The extension of MPC to systems with periodic characteristics, referred to as periodic

* Corresponding author.
E-mail address: xiexiaochen@hit.edu.cn (X. Xie).

https://doi.org/10.1016/j.jfranklin.2025.108358
Received 11 July 2025; Received in revised form 13 November 2025; Accepted 13 December 2025
Available online 17 December 2025

MPC (P-MPC), has been explored in studies such as [17]. More recently, the integration of discrete-time CBFs (DCBFs) with MPC has gained significant attention [18], known as MPC-DCBF, where DCBFs are incorporated in a rolling-horizon mode to enforce safety constraints. Building on this, Liu et al. [19] introduced an iterative convex optimization framework for MPC with discrete-time HOCBFs (DHOCBFs). The MPC-DCBF has been successfully applied to various domains, including lane merging [20], autonomous driving [21], and legged robots [22]. However, as discussed in [23], the trade-off between safety and feasibility remains an open challenge, motivating further research in this direction.

In recent years, the field of bipedal robotics has witnessed remarkable advancements. Various modeling approaches have been proposed for bipedal robots, among which the variable-height inverted pendulum (VHIP) model extends the linear inverted pendulum (LIP) model by incorporating vertical center-of-mass (CoM) motion, thereby accurately capturing the dynamics of human locomotion [24]. The CoM height can be constrained by time-dependent trajectories [25], or by some spatial manifolds [26]. Given the inherent periodicity of bipedal walking, such a motion can naturally be represented as system states with periodic characteristics, which attracts our attention. Several works have explored periodic gait generation, such as [27], which proposed an approach to generate periodic reference trajectories for bipedal robots, and [28], which considered a periodic gait represented as a sum of sine harmonics. Additionally, the problem of maintaining periodic walking while tracking planned trajectories has been investigated in [29].

From a practical perspective, ensuring safety in bipedal robotic systems is of paramount importance [30], encompassing various aspects such as obstacle avoidance [31] and self-collision prevention [32]. However, traditional CBF formulations tend to be overly conservative when applied to safety-critical control in periodic walking scenarios. This observation motivates us to develop a novel CBF specifically designed for systems that exhibit periodic characteristics in their states. The key contributions of this work are summarized as follows:

1. Innovatively considering the safety issues of systems with periodic characteristics in system states, we develop the concept of P-DHOCBF, which is integrated into P-MPC to formulate an optimization-based control strategy.
2. The periodic characteristics of the state are abstracted from the gait period of the bipedal robot, which is also used to derive relevant constraints for the optimization problem.
3. Comparative simulations based on a 12-DOF bipedal robot demonstrate the superior capability of P-DHOCBF in ensuring safety while reducing conservatism, which is also quantitatively assessed by introducing a safety margin ratio for a more precise presentation.

The paper is organized as follows. Section 2 gives the theoretical preliminaries and formulates the safety control problem. Section 3 gives the main results of P-DHOCBF and a simulation example. Section 4 gives the P-MPC framework combined with P-DHOCBF. Section 5 presents the modeling of the bipedal robot and the derivation of related constraints. The effectiveness of the proposed method is verified through comparative simulation and analysis. Section 6 concludes the paper.

Notation: $\mathbb{R}^n$ denotes the n-dimensional Euclidean space. $\mathbb{N}$ denotes the set of natural numbers (including zero). $\mathcal{X}$ denotes a closed-state constraint set. $\mathcal{U}$ denotes a closed-control constraint set.

2. Problem formulation and preliminaries

Before starting our work, it is necessary to take a brief introduction to recall the existing DHOCBF. Above all, some necessary preliminaries are presented below.

Consider a discrete-time system:

$$\mathbf{x}(k+1) = f(\mathbf{x}(k), \mathbf{u}(k)), \tag{1}$$

where $\mathbf{x}(k) \in \mathcal{X} \subset \mathbb{R}^{n_x}$ represents the system state at time step k, $\mathbf{u}(k) \in \mathcal{U} \subset \mathbb{R}^{n_u}$ is the control input, and the function f is locally Lipschitz. Furthermore, the safety set of system (1) is given as $C = \{\mathbf{x} \in \mathbb{R}^{n_x} : h(\mathbf{x}) \geq 0\}$, where $h : \mathbb{R}^{n_x} \to \mathbb{R}$ is a continuous function that, in practical discrete-time implementations, may be sampled at discrete time steps $k \in \mathbb{N}$.

Definition 1 (Relative degree [33]). For system (1), the relative degree m of function h means the required steps (delay) for control input $\mathbf{u}(k)$ to show explicitly in h.

Definition 2 (Forward invariance [12]). If for any initial condition $x(0) \in C$ and any $k \geq 0$, the solution of system (1) always holds that $\mathbf{x}(k) \in C$, then set C is said to be forward invariant.

Next, assume that $h(\mathbf{x}(k))$ has relative degree m to system (1). Define a family of functions $\psi_i : \mathbb{R}^n \to \mathbb{R}, i = 1, \dots, m-1$, as follows:

$$\psi_m(\mathbf{x}(k), \mathbf{u}(k)) := \Delta\psi_{m-1}(\mathbf{x}(k), \mathbf{u}(k)) + \alpha_m(\psi_{m-1}(\mathbf{x}(k))), \tag{2a}$$
$$\psi_i(\mathbf{x}(k)) := \Delta\psi_{i-1}(\mathbf{x}(k)) + \alpha_i(\psi_{i-1}(\mathbf{x}(k))), \tag{2b}$$
$$\psi_0(\mathbf{x}(k)) := h(\mathbf{x}(k)), \tag{2c}$$
$$\Delta\psi_{i-1}(\mathbf{x}(k)) := \psi_{i-1}(\mathbf{x}(k+1)) - \psi_{i-1}(\mathbf{x}(k)), \tag{2d}$$

where $\alpha_i(\cdot)$ are class $\mathcal{K}$ functions, and functions $\psi_0, \psi_1, \dots, \psi_{m-1}$ depend solely on the state $\mathbf{x}(k)$ due to the relative degree m. The control input $\mathbf{u}(k)$ appears explicitly only in ψ_m, allowing $\mathbf{u}(k)$ to constrain the system state $\mathbf{x}(k)$ through constraints based on ψ_m, thereby ensuring safety.

In this case, the safety sets C_i are defined as follows:

$$C_i(k) := \{\mathbf{x}(k) : \psi_i(\mathbf{x}(k)) \geq 0\}, \quad i = 0, 1, \dots, m-1. \tag{3}$$

Remark 1. The safety set $C_i(k)$ is defined as a subset of the state space, representing the constraints that the system state must satisfy. Its definition does not depend on state $\mathbf{x}$, but is affected by dynamic obstacles whose properties change over time.

Definition 3 (DHOCBF [34])**.** According to (2), if there exists a function $\psi_m(\mathbf{x}(k), \mathbf{u}(k))$ and a control input $\mathbf{u}(k)$ such that

$$\psi_m(\mathbf{x}(k), \mathbf{u}(k)) \geq 0, \quad \forall \mathbf{x}(k) \in C_0 \cap \cdots \cap C_{m-1}, \tag{4}$$

then function $h : \mathbb{R}^{n_x} \to \mathbb{R}$ is said to be a DHOCBF with relative degree m for system (1).

Given a DHOCBF $h(\mathbf{x}(k))$ and initial condition $\mathbf{x}(0) \in C_0(0) \cap \cdots \cap C_{m-1}(0)$, any discrete-time controller $\mathbf{u}(k)$ satisfying (4) makes the safety set $C_0(k) \cap \cdots \cap C_{m-1}(k)$ of system (1) forward invariant for any $k \geq 0$, that is, $\mathbf{x}(k) \in C_0(k) \cap \cdots \cap C_{m-1}(k)$, $\forall k \geq 0$ (see [34] for details).

So far, we have concisely reviewed the issues related to DHOCBF. Next, we provide definitions of the conservatism of safety, the safety margin, and the safety margin ratio.

Definition 4 (Conservatism of Safety)**.** The conservatism of safety refers to the over-restrictiveness of the safety constraints imposed on the system, that is, the state is maintained at a larger-than-necessary distance from the safety boundary.

Definition 5 (Safety Margin and Safety Margin Ratio)**.** Under control barrier function $h(\mathbf{x}(k))$, the average safety margin of the state $\mathbf{x}(k)$ is defined as

$$\bar{h} = \frac{1}{N_0} \sum_{k=1}^{N_0} h(\mathbf{x}(k)), \tag{5}$$

where N_0 is the total length of the data. Then, the ratio of the safety margins between two different control barrier functions h_1 and h_2 is defined as the safety margin ratio M, that is,

$$M = \frac{\bar{h}_1}{\bar{h}_2} \times 100\,\%, \tag{6}$$

where $M < 1$, $M = 1$, and $M > 1$ respectively imply that the safety conservatism of h_1 is smaller than, equal to, and greater than that of h_2.

Remark 2. Similar indicators involving safety margins have been explored in the CBF literature, such as [35,36]. While these concepts also quantify the conservatism of safety, our approach specifically emphasizes comparing the safety margins of different CBFs.

Assumption 1. Assume the state $\mathbf{x}(k)$ of system (1) has a time period N, that is,

$$\mathbf{x}(k) = \mathbf{x}(k + \ell N), \tag{7}$$

where N is the minimum integer for which (7) is satisfied, and $\ell \in \mathbb{N}$.

Next, we will formulate the safety problem for discrete-time systems with periodic characteristics in system states.

Problem 1. The goal is to construct a periodic safety set based on the periodicity in the system, thereby designing a periodic DHOCBF as needed. Then, design a discrete-time controller to ensure that $\mathbf{x}(k)$ has a time period N and system (1) is safe, while reducing the conservatism of safety.

3. Periodic discrete-time high-order control barrier function

3.1. Concept proposal and theoretical derivation

Under the periodicity condition (7), we consider a class of super-level sets C_i, $i = 0, 1, \dots, m-1$, defined as the safety sets of system (1). The safety sets C_i exhibit a time period N, that is,

$$C_i(k) = C_i(k + \ell N), \quad i = 0, 1, \dots, m-1. \tag{8}$$

The specific forms of C_i are

$$C_i(k + \ell N) := \{\mathbf{x}(k + \ell N) : \psi_i(\mathbf{x}(k + \ell N)) \geq 0\}, \quad i = 0, 1, \dots, m-1. \tag{9}$$

Then we can express the above safety sets as

$$C(k + \ell N) = \bigcap_{i=0,1,\dots,m-1} C_i(k + \ell N). \tag{10}$$

Next, we are going to present the concept and definition of our P-DHOCBF and build the forward invariance of the periodic safety set. Suppose that there is a family of functions with the following form:

$$\psi_0(\mathbf{x}(k+\ell N)) := h(\mathbf{x}(k+\ell N)), \tag{11a}$$

$$\psi_i(\mathbf{x}(k+\ell N)) := \psi_{i-1}(\mathbf{x}(k+1+\ell N)) - \psi_{i-1}(\mathbf{x}(k+\ell N)) + \alpha_i^{\ell}(\psi_{i-1}(\mathbf{x}(k+\ell N))), \tag{11b}$$

$$\psi_m(\mathbf{x}(k+\ell N), \mathbf{u}(k+\ell N)) := \psi_{m-1}(\mathbf{x}(k+1+\ell N)) - \psi_{m-1}(\mathbf{x}(k+\ell N)) + \alpha_m^{\ell}(\psi_{m-1}(\mathbf{x}(k+\ell N))), \tag{11c}$$
$$i = 1, 2, \dots, m-1, \quad k = 0, 1, \dots, N-1,$$

where $\alpha_i^{\ell}(\cdot)$ denotes the class $\mathcal{K}$ functions defined in the periodic interval $[0+\ell N, N-1+\ell N], \ell \in \mathbb{N}$. It is obvious that $h(\mathbf{x}(k))$ and $\psi_i(\mathbf{x}(k))$ satisfying (20c) and (11b) have a time period N that is equal to the system period, that is,

$$\psi_i(\mathbf{x}(k)) = \psi_i(\mathbf{x}(k+\ell N)), \quad i = 0, 1, \dots, m. \tag{12}$$

Then, according to the periodicity of $\psi_i(\mathbf{x}(k))$, $i = 0, 1, \dots, m$, we can conclude that $\alpha_i^{\ell}(\psi_{i-1}(\mathbf{x}(k+\ell N)))$ are periodic functions, that is,

$$\alpha_i^{\ell}(\psi_{i-1}(\mathbf{x}(k+\ell N))) = \alpha_i^{\ell+1}(\psi_{i-1}(\mathbf{x}(k+(\ell+1)N))), \quad i = 1, 2, \dots, m, \quad \ell \in \mathbb{N}. \tag{13}$$

Hence, in the following text, we will refer to $\alpha_i^{\ell}(\cdot)$ as $\alpha_i(\cdot)$.

Definition 6 (P-DHOCBF)**.** If there exists a family of periodic functions $\psi_i(\mathbf{x}(k))$, $i \in \{0, \dots, m\}$, defined as in (11) and a periodic controller $\mathbf{u}(k+\ell N)$, such that

$$\psi_m(\mathbf{x}(k+\ell N), \mathbf{u}(k+\ell N)) \geq 0, \tag{14}$$

for $\forall \mathbf{x}(k+\ell N) \in C(k+\ell N)$ is satisfied, then $h : \mathbb{R}^{n_x} \to \mathbb{R}$ is said to be a P-DHOCBF for system (1).

Lemma 1 (adapted from [37])**.** *Consider a discrete-time function $b(k) : \mathbb{N} \to \mathbb{R}$. If for any $k \in \mathbb{N}$, $b(k+1) - b(k) \geq -\alpha(b(k))$ always holds, where α is a class $\mathcal{K}$ function and $b(0) \geq 0$, then we can get $b(k) \geq 0$.*

Theorem 1. *If $h(\mathbf{x}(k))$ is a P-DHOCBF with relative degree $m \geq 2$, then any discrete-time periodic controller $\mathbf{u}(k)$ which satisfies (7) and (14) ensures the forward invariance of the periodic safety set $C(k+\ell N)$ with respect to system (1).*

Proof. For convenience, only one time period $[0, N-1]$ is considered here, and the condition in other periods can be obtained similarly. If $h(\mathbf{x}(k))$ is a P-DHOCBF, then based on Definition 6, we can conclude that $\psi_m(\mathbf{x}(k), \mathbf{u}(k)) \geq 0$ holds for any time k, $k \in [0, N-1]$, that is,

$$\psi_{m-1}(\mathbf{x}(k+1)) - \psi_{m-1}(\mathbf{x}(k)) + \alpha_m(\psi_{m-1}(\mathbf{x}(k))) \geq 0.$$

Since $\mathbf{x}(0) \in C(0)$, then $\mathbf{x}(0) \in C_{m-1}(0)$, that is, $\psi_{m-1}(\mathbf{x}(0)) \geq 0$. Applying Lemma 1 to the discrete-time function $k \mapsto \psi_{m-1}(\mathbf{x}(k))$, we can obtain that $\psi_{m-1}(\mathbf{x}(k)) \geq 0$ satisfies for any time $k \in [0, N-1]$, that is,

$$\psi_{m-2}(\mathbf{x}(k+1)) - \psi_{m-2}(\mathbf{x}(k)) + \alpha_{m-1}(\psi_{m-2}(\mathbf{x}(k))) \geq 0.$$

Also we have $\mathbf{x}(0) \in C_{m-2}(0)$, again in the light of Lemma 1, there is $\psi_{m-2}(\mathbf{x}(k)) \geq 0$ for any time $k \in [0, N-1]$.

According to (9), repeat the above process continuously, and we will eventually acquire $\mathbf{x}(k) \in C_i(k)$, $i \in \{0, 1, \dots, m-1\}$, for any time k, $k \in [0, N-1]$. According to the periodicity of $C(k)$, the safety set $C(k+\ell N)$ is forward invariant. □

Remark 3. Here we define the high-order form directly and omit the first-order form because it can be obtained by setting $m = 1$ in P-DHOCBF, that is, $h(\mathbf{x}(k+1+\ell N)) - h(\mathbf{x}(k+\ell N)) \geq -\alpha(h(\mathbf{x}(k+\ell N)))$.

3.2. Example: Van der Pol oscillator

To provide readers with a clearer understanding of the usage and effectiveness of our proposed P-DHOCBF, we present an illustrative example: the classical Van der Pol oscillator [38]. The limit cycle oscillation is expressed as

$$\frac{\mathrm{d}^2 x}{\mathrm{d}t^2} - \beta(1-x^2)\frac{\mathrm{d}x}{\mathrm{d}t} + x = 0. \tag{15}$$

Then, we introduce a control input u to constrain the state variables, and discretize the system to obtain the following state-space form:

$$\begin{cases} x_1(k+1) = x_1(k) + x_2(k)\delta, \\ x_2(k+1) = x_2(k) + (\beta x_2(k) - x_1(k) - \beta x_1^2(k) x_2(k) + u(k))\delta, \end{cases} \tag{16}$$

where δ is the sampling interval.

When $\beta = 0$, x_1 and x_2 oscillate with constant amplitudes, that is,

$$x_1(k) = x_1(k+\ell N), \quad x_2(k) = x_2(k+\ell N). \tag{17}$$

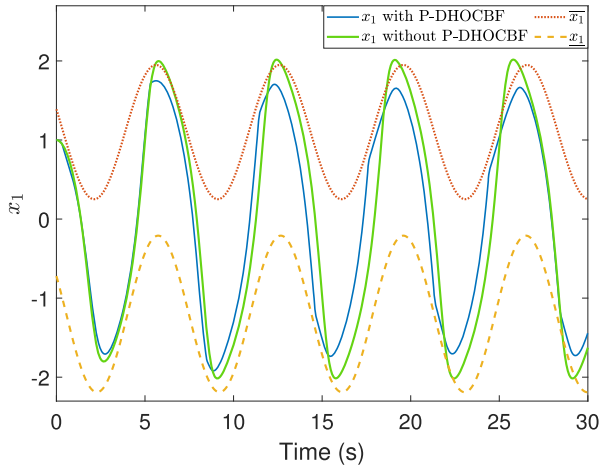

(a) x_1 with and without P-DHOCBF

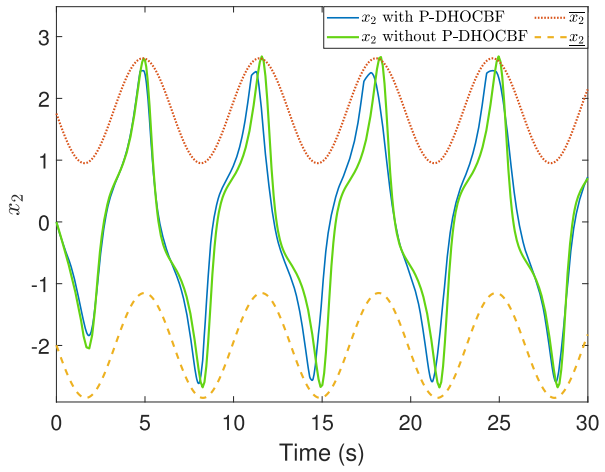

(b) x_2 with and without P-DHOCBF

Fig. 1. Harmonic oscillations of the Van der Pol oscillator with and without P-DHOCBF constraints.

In many cases, it is required to limit x_1 and x_2 within certain ranges, where our P-DHOCBF can play an effective role in a concise form. Here, assuming that $x_1(k)$ and $x_2(k)$ need to be constrained within the periodic maximum and minimum safety boundaries, that is, $\underline{x_1}(k) < x_1(k) < \overline{x_1}(k)$ and $\underline{x_2}(k) < x_2(k) < \overline{x_2}(k)$, then the P-DHOCBFs are

$$\overline{h_1}(x_1,k) = \overline{x_1}(k) - x_1(k), \quad \underline{h_1}(x_1,k) = x_1(k) - \underline{x_1}(k), \tag{18a}$$

$$\overline{h_2}(x_2,k) = \overline{x_2}(k) - x_2(k), \quad \underline{h_2}(x_2,k) = x_2(k) - \underline{x_2}(k), \tag{18b}$$

wherein $\underline{x_1}(k)$, $\overline{x_1}(k)$, $\underline{x_2}(k)$ and $\overline{x_2}(k)$ are respectively constructed based on the periodicity of x_1 and x_2. Like this, we can see that $\overline{h_1}(x_1,k)$ and $\underline{h_1}(x_1,k)$ have a relative degree 2, while $\overline{h_2}(x_2,k)$ and $\underline{h_2}(x_2,k)$ have a relative degree 1.

The simulation results are shown in Fig. 1, where the system states are depicted as continuous trajectories for visual clarity, although they are obtained from discrete-time system (16) with a sampling interval of $\delta = 0.01$ s. It can be seen that P-DHOCBF constraints have restricted both x_1 and x_2 within our designated safety zones, effectively ensuring the safety of system (16).

4. P-MPC with P-DHOCBF

In this section, we integrate P-DHOCBF with MPC to give a framework for the optimization problem. Since MPC explicitly takes constraints into account, it is appropriate to be chosen to implement a constrained control problem. The general idea of MPC is to solve the optimal control problem at each time k online based on the measured state $\mathbf{x}(k)$, repeatedly. Due to the periodicity of the

state in (7), P-MPC is taken into consideration. A quadratic cost function with a finite prediction horizon H is denoted as

$$J(\mathbf{x}(k),\mathbf{u}(k)) = \mathbf{x}^T(k+H|k)P_{k+H}\mathbf{x}(k+H|k) + \sum_{i=0}^{H-1}(\mathbf{x}^T(k+i|k)Q\mathbf{x}(k+i|k) + \mathbf{u}^T(k+i|k)R\mathbf{u}(k+i|k)), \tag{19}$$

where the weighting matrices $Q \in \mathbb{R}^{n_x \times n_x}$, $R \in \mathbb{R}^{n_u \times n_u}$ and the terminal penalty matrix $P_{k+H} \in \mathbb{R}^{n_x \times n_x}$ are all positive definite. And the control input trajectory is represented by the sequence $\mathbf{u}(k) = [\mathbf{u}(k|k), \mathbf{u}(k+1|k), \dots, \mathbf{u}(k+H-1|k)]$. Hence, the optimal control problem constructed by the P-MPC method is as follows:

$$\min_{\mathbf{u}(k)} \quad J(\mathbf{x}(k),\mathbf{u}(k)) \tag{20a}$$

$$\text{s.t.} \quad \mathbf{x}(k+i|k) \in \mathcal{X},\ \mathbf{u}(k+i|k) \in \mathcal{U}, \tag{20b}$$

$$\mathbf{x}(k|k) = \mathbf{x}(k), \tag{20c}$$

$$\psi_m(\mathbf{x}(k+i|k)) \geq 0, \tag{20d}$$

$$\phi(\mathbf{x}(k+i|k)) \geq\ 0, i = 0, 1, \dots, H-1, \tag{20e}$$

$$\mathbf{x}(k+H|k) \in \mathcal{X}_{f,k+H}. \tag{20f}$$

In the above formulas, index $k+i|k$ represents the time variable of the predicted value at prediction time $k+i$, where the prediction is calculated at the current time k. In detail, $\mathbf{x}(k+i|k)$ means the predicted state vector at time $k+i$ obtained by applying the control input $\mathbf{u}(k:k+H-1|k)$ to the system (1) starting from the current state $\mathbf{x}(k)$.

The state constraint and input constraint are given by (20b), and the initial condition is given by (20c). The P-DHOCBF constraints are denoted as (20d). In addition, the remaining constraints denoted as $\phi(\mathbf{x}(k+i|k))$ are compactly represented by (20e). The terminal constraint is enforced in (20f), meaning that the state at the end of the prediction, $\mathbf{x}(k+H|k)$, is forced to lie within the terminal region $\mathcal{X}_{f,k+H}$. Further, according to the periodicity of the system, the following periodic constraints can be presented as

$$\mathcal{X}_{f,k+H} = \mathcal{X}_{f,k+H+\ell N}, \quad \mathbf{u}(k) = \mathbf{u}(k+\ell N), \tag{21}$$

which show a significant difference between the P-MPC and the ordinary form.

At each time step k, the first part of the obtained optimal input sequence $\mathbf{u}^*(k) = \arg\min_{\mathbf{u}(k)} J(\mathbf{x}(k),\mathbf{u}(k))$ is selected to be applied to the system input, which will be used to get the newly calculated $\mathbf{x}(k+1)$. Similarly, by repeating the optimal control pattern (20b) at time $k+1$, a rolling optimization strategy is generated to obtain the control input values.

5. Bipedal robot simulation verification

In our work, we are interested in bipedal robots as they are ideal examples of dynamic systems that exhibit a periodic motion structure during gait behaviors. In this section, we will consider modeling the bipedal robot with periodic forward walking. Also, constraints related to robot walking will be derived and incorporated into the P-MPC formula to obtain a quadratic programming problem, which will be verified through simulation later.

5.1. Bipedal robot modeling

We model the bipedal robot based on the VHIP model. To be specific, when the bipedal robot supports its body with one leg and the other leg is in the swinging process, its dynamics can be represented by an inverted pendulum connecting the supporting leg and the Center of Mass (CoM) of the robot [39]. The schematic diagram of the bipedal robot based on VHIP modeling is shown in Fig. 2. The positions of the CoM and the Zero Moment Point (ZMP) of the bipedal robot are indicated by $(x_{com}, y_{com}, z_{com})$ and $(x_{zmp}, y_{zmp}, 0)$, respectively.

In this way, a VHIP model of the bipedal robot walking can be acquired [40], which has decoupled x-axis, y-axis, and z-axis dynamics with similar forms as

$$\ddot{x}_{com} = \eta(x_{com} - x_{zmp}), \tag{22a}$$

$$\ddot{y}_{com} = \eta(y_{com} - y_{zmp}), \tag{22b}$$

$$\ddot{z}_{com} = \eta(z_{com} - z_{zmp}) - g, \tag{22c}$$

where $\eta = (\ddot{z}_{com} + g)/z_{com}$, g is the gravity acceleration and z_{com} is the height of the robot's CoM. Letting $v^x_{com} \triangleq \dot{x}_{com}$, discretize the system using the Euler method and consider that the robot moves along the x-axis on a flat horizontal ground. For the sake of simplicity, here we only take the x-axis direction as an example, and x_{zmp} is selected as the system control input. Thereupon, we can get the following dynamic model:

$$\begin{pmatrix} x_{com}(k+1) \\ v^x_{com}(k+1) \end{pmatrix} = \underbrace{\begin{pmatrix} 1 & \delta \\ \eta\delta & 1 \end{pmatrix}}_{A(k)} \begin{pmatrix} x_{com}(k) \\ v^x_{com}(k) \end{pmatrix} + \underbrace{\begin{pmatrix} 0 \\ -\eta\delta \end{pmatrix}}_{B(k)} x_{zmp}(k), \tag{23}$$

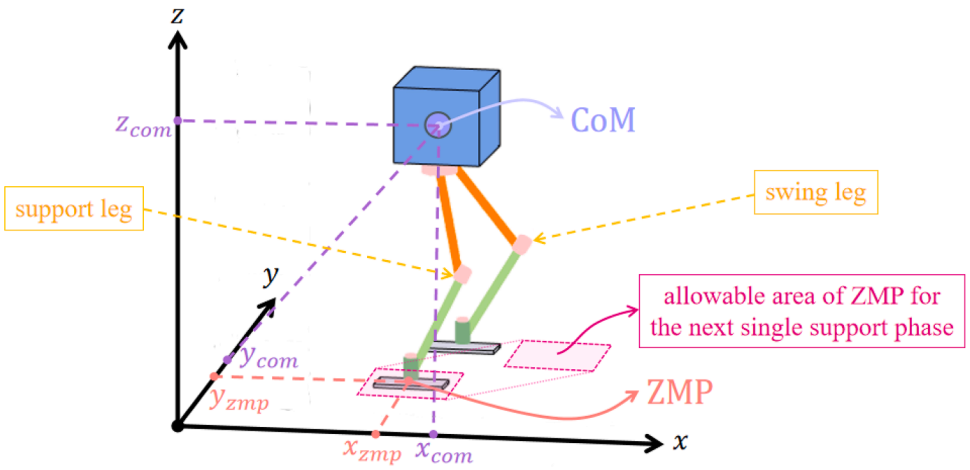

Fig. 2. Schematic diagram of the bipedal robot based on VHIP modeling.

where δ is the sampling interval. Considering the periodic forward walking problem of the bipedal robot, it can be obtained that $v^x_{com}(k)$ has a time period N, which is the gait period.

Next, a 12-DOF bipedal robot (6 DOFs per leg: 3 DOFs at the hip, 1 DOF at the knee, and 2 DOFs at the ankle) is constructed. Based on the CoM and foot positions solved by MPC, the rotation angles of the legs can be obtained based on inverse kinematics (IK). After that, all links' global positions and postures can be calculated using forward kinematics (FK). In this way, the forward walking of the bipedal robot can be realized.

As introduced in [41], to avoid the generation of nonlinear systems, we predefine a periodic function which describes the vertical motion of CoM. For the sake of obtaining a motion trajectory with human-like CoM, the vertical motion of CoM is selected as a cosine trajectory, as shown below:

$$z_{com}(k) = Z_{com} + \Delta_z \cos(2\pi k/N), \tag{24}$$

where Z_{com} is the nominal CoM height, and Δ_z is the amplitude of the height change of the CoM during the robot's walking process. The vertical motion of CoM has a period N, which is also the gait period.

Remark 4. Similar to the approach in [42], in simulation, the N-periodic and piecewise ZMP speed v^x_{zmp} is utilized as the actual input, which is constant in each sampling interval. Moreover, in each sampling interval, a piecewise linear continuous system control input x_{zmp} can be obtained.

5.2. P-DHOCBF constraints

In the following, we will impose a range constraint on the velocity of the robot's CoM, that is, $v^x_{com}(k) \le \overline{V}_{P-DHOCBF}(k)$, and construct a CBF based on that. It is easy to find out that the relative degree of this problem is 1, and the exact form is as follows:

$$h_{P-DHOCBF}(k, v^x_{com}(k)) = \overline{V}_{P-DHOCBF}(k) - v^x_{com}(k). \tag{25}$$

Thus, depending on Definition 6, we have

$$\psi_1(k + \ell N, v^x_{com}(k + \ell N)) \ge 0. \tag{26}$$

Here, $\overline{V}_{P-DHOCBF}(k)$ is designed as a periodic function, that is, $\overline{V}_{P-DHOCBF}(k) = \overline{V}_{P-DHOCBF}(k + \ell N)$, $\ell \in \mathbb{N}$, which accurately fits the gait period. The above P-DHOCBFs $\psi_0(k + \ell N, v^x_{com}(k + \ell N))$ and $\psi_1(k + \ell N, v^x_{com}(k + \ell N))$ share the same time period N, which is an essential difference between the P-DHOCBF and the traditional DCBF. Namely, the periodic characteristic of robot system (23) is utilized to construct a periodic safety set, thereby obtaining the required P-DHOCBF.

5.3. Zero moment point constraints

Consider the minimum polygonal area, which can accommodate all contact points between the sole of a bipedal robot and the ground, called the supporting polygon (that is, the allowable area for ZMP). The robot can maintain balance if the ZMP position is strictly within the supporting polygon. Otherwise, the robot will flip over if the ZMP position goes outside the supporting polygon [39].

When the robot is in the single support state of step l, the allowable area for ZMP can be approximated as a rectangle with dimensions $x_{zmp(\max)}(k + l)$ and $y_{zmp(\max)}(k + l)$, centered at $(x_{st}(k + l), y_{st}(k + l))$, as shown in Fig. 3. Simply put, the constraint for $l \in [1, H]$ in the x- and y-axis can be denoted as

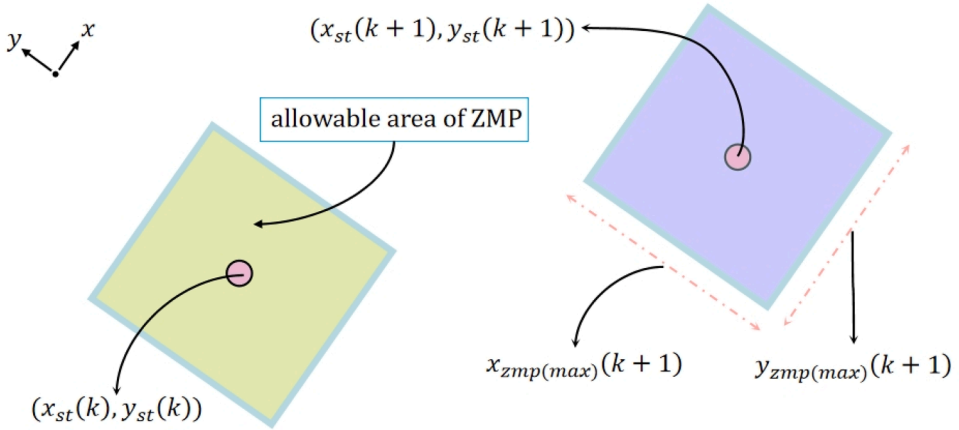

Fig. 3. Schematic diagram of ZMP.

$$x_{zmp}(k+l) - x_{st}(k+l) \geq -\frac{x_{zmp(\max)}(k+l)}{2}, \tag{27a}$$

$$x_{zmp}(k+l) - x_{st}(k+l) \leq \frac{x_{zmp(\max)}(k+l)}{2}, \tag{27b}$$

$$y_{zmp}(k+l) - y_{st}(k+l) \geq -\frac{y_{zmp(\max)}(k+l)}{2}, \tag{27c}$$

$$y_{zmp}(k+l) - y_{st}(k+l) \leq \frac{y_{zmp(\max)}(k+l)}{2}. \tag{27d}$$

Remark 5. The detailed derivation process related to ZMP can be found in [43]. Since the focus of this study is on P-DHOCBF, we omit the deduction for (27a), giving the final conclusion directly.

5.4. Stability constraint and terminal constraint

Due to the inherent instability of VHIP dynamics [44], even if the ZMP constraint is always satisfied, it is still possible for the CoM to diverge exponentially relative to the ZMP. In this paper, inspired by [45], we resort to an equality stability constraint on MPC to ensure that the generated CoM trajectory remains bounded relative to the ZMP. Here, we borrow the conclusions of stability constraint (28) and terminal constraint (29) from [45]:

$$\sum_{i=0}^{H-1} e^{-i\eta\delta} v^x_{zmp}(k+i) = -\sum_{i=H}^{\infty} e^{-i\eta\delta} v^x_{zmp}(k+i) + \frac{\eta}{1-e^{-\eta\delta}}(x_u(k) - x_{zmp}(k)), \tag{28}$$

$$x_u(k+H) = x_{zmp}(k+H) + \frac{1-e^{-\eta\delta}}{\eta} e^{H\eta\delta} \sum_{i=H}^{\infty} e^{-i\eta\delta} v^x_{zmp}(k+i). \tag{29}$$

where x_u is the unstable component, also known as the motion divergence component or capture point. Specifically, we decompose LIP dynamics into stable subsystem x_s and unstable subsystem x_u through the following coordinate transformation:

$$x_u = x_{com} + \frac{v^x_{com}}{\eta}, \tag{30a}$$

$$x_s = x_{com} - \frac{v^x_{com}}{\eta}. \tag{30b}$$

Then, recast the above equations to attain

$$\dot{x}_u = \eta\left(x_u - x_{zmp}\right), \tag{31a}$$

$$\dot{x}_s = -\eta\left(x_s - x_{zmp}\right). \tag{31b}$$

The stability constraint and terminal constraint are related to $v^x_{zmp}(k+H), v^x_{zmp}(k+H+1), \ldots$, which are the ZMP velocities after the prediction horizon. Therefore, this is a physically unrealizable system controller. Logically, next, we will consider how to obtain

a realizable system controller. It is natural to give these ZMP velocities some suitable guess values, making the stability constraints achievable.

We use the system's periodicity to speculate on the unknown ZMP velocities after the prediction horizon, denoted as $\tilde{v}^x_{zmp}(k+H), \tilde{v}^x_{zmp}(k+H+1), \ldots$. To deal with the periodicity, we choose the method mentioned in [46]. Specifically, if the prediction horizon H is chosen as the gait period (the total duration of two consecutive steps) or a multiple of it, this problem can be simplified. The following lemma is given.

Lemma 2. *Let the predicted ZMP velocities $\tilde{v}^x_{zmp}(k+H)$, $\tilde{v}^x_{zmp}(k+H+1), \ldots,$ have a time period H, that is,*

$$\tilde{v}^x_{zmp}(k+i) = \begin{cases} v^x_{zmp}(k+i-H), i = H, \ldots, 2H-1, \\ \tilde{v}^x_{zmp}(k+i-H), i \geq 2H. \end{cases} \tag{32}$$

Then, the stability constraint and the terminal constraint can be modified to the following forms:

$$\sum_{i=0}^{H-1} e^{-i\eta\delta} v^x_{zmp}(k+i) = \eta \frac{1-e^{-H\eta\delta}}{1-e^{-\eta\delta}} (x_u(k) - x_{zmp}(k)), \tag{33}$$

$$v^x_u(k+H) = v^x_u(k). \tag{34}$$

Proof. To start with, let $\zeta = i - H$, which leads to

$$\begin{aligned} &\sum_{i=H}^{\infty} e^{-i\eta\delta} \tilde{v}^x_{zmp}(k+i) \\ &= \sum_{\zeta=0}^{\infty} e^{-(\zeta+H)\eta\delta} \tilde{v}^x_{zmp}(k+H+(\zeta+H)) \\ &= e^{-H\eta\delta} \sum_{\zeta=0}^{\infty} e^{-\zeta\eta\delta} \tilde{v}^x_{zmp}(k+H+\zeta) \\ &= \frac{e^{-H\eta\delta}}{1-e^{-H\eta\delta}} \sum_{\zeta=0}^{H-1} e^{-\zeta\eta\delta} v^x_{zmp}(k+\zeta). \end{aligned} \tag{35}$$

Stability constraint: By substituting (35) into stability constraint (28), it is straightforward to come by

$$\sum_{i=0}^{H-1} e^{-i\eta\delta} v^x_{zmp}(k+i) = -\frac{e^{-H\eta\delta}}{1-e^{-H\eta\delta}} \sum_{i=0}^{H-1} e^{-i\eta\delta} v^x_{zmp}(k+i) + \frac{\eta}{1-e^{-\eta\delta}} (x_u(k) - x_{zmp}(k)).$$

Further, processing of the above equation yields

$$\sum_{i=0}^{H-1} e^{-i\eta\delta} v^x_{zmp}(k+i) = \frac{\eta(1-e^{-H\eta\delta})}{1-e^{-\eta\delta}} (x_u(k) - x_{zmp}(k)).$$

Terminal constraint: Similarly, substituting (35) into (29) yields

$$x_u(k+H) - x_{zmp}(k+H) = \frac{1-e^{-\eta\delta}}{\eta} \cdot \frac{1}{1-e^{-H\eta\delta}} \sum_{i=0}^{H-1} e^{-i\eta\delta} v^x_{zmp}(k+i).$$

Then, using the proven stability constraint (33), it can be concluded that

$$x_u(k+H) - x_{zmp}(k+H) = x_u(k) - x_{zmp}(k).$$

Afterwards, on account of $v^x_u(k) = \eta\big(x_u(k) - x_{zmp}(k)\big)$, we get hold of $x_{zmp}(k+H) = x_u(k+H) - v^x_u(k+H)/\eta$. As a result, the terminal constraint can be represented as $v^x_u(k+H) = v^x_u(k)$. □

Remark 6. It is worth noting that the terminal constraint $v^x_u(k+H) = v^x_u(k)$ exhibits a time period H. With the earlier assumption $H = \omega N, \omega = 1, 2, \ldots$, this design exploits the periodicity of the system, which also reflects the characteristics of the periodic control method proposed in this paper.

5.5. Formulation of the optimization problem

Based on the above analysis, we propose the following P-MPC formulation using our P-DHOCBF:

$$\begin{aligned} \min_{V^x_{st}(k), V^y_{st}(k), X_{zmp}(k), Y_{zmp}(k)} \quad & \|V^x_{zmp}(k)\|^2 + \|V^y_{zmp}(k)\|^2 + \varepsilon\big(\|X_{st} - X^*_{st}\|^2 + \|Y_{st} - Y^*_{st}\|^2\big) \\ \text{s.t.} \quad & (26),\ (27),\ (33),\ (34), \end{aligned} \tag{36}$$

where subscript st refers to variables related to the standing foot, and

$$V^x_{zmp}(k) = [v^x_{zmp}(k), \ldots, v^x_{zmp}(k+H-1)]^T, \tag{37a}$$

$$V^{y}_{zmp}(k) = [v^{y}_{zmp}(k), \dots, v^{y}_{zmp}(k+H-1)]^T, \tag{37b}$$

$$X_{st}(k) = [x_{st}(k+1), \dots, x_{st}(k+H)]^T, \tag{37c}$$

$$Y_{st}(k) = [y_{st}(k+1), \dots, y_{st}(k+H)]^T. \tag{37d}$$

In (36), X^*_{st}, Y^*_{st} are the expected x-axis and y-axis position of the standing foot; ϵ is a scalar weight of the quadratic term $\left(\|X_{st} - X^*_{st}\|^2 + \|Y_{st} - Y^*_{st}\|^2\right)$, which is used to penalize the deviation of the standing foot positions relative to the expected ones.

Remark 7. In practice, actuation is subjected to constraints on joint torques, velocities, etc. Although not explicitly modeled in our current formulation, these constraints can be embedded into P-MPC via box constraints or rate limiters on the joint space control inputs.

Remark 8. When applied in real-world bipedal platforms, the CoM position and velocity are estimated using an IMU combined with FK from joint encoders. The ZMP position is computed from foot-mounted force/torque sensors. The current foot placement is reconstructed via FK, and the resulting states are passed to the controller. At each control cycle, the controller solves the optimization problem. The resulting reference CoM and foot trajectories are then transformed into joint commands via IK. Finally, low-level position/torque controllers execute these commands, while feedback from encoders and sensors ensures closed-loop tracking.

5.6. Simulation verification and discussion

We verify the effectiveness of our approach through simulation based on the considered bipedal robot. The nominal CoM height of the 12-DOF bipedal robot is 0.58 m, and the side length of the ZMP allowable region is designed to be 0.1 m. All simulation results for the robot system are presented with a continuous line plot for visual clarity, with a sampling interval of $\delta = 0.01$ s. Moreover, without loss of generality, we take $\alpha_1 = 1$ in DCBF and P-DHOCBF.

In addition, the prediction horizon H is chosen to be 80 (that is, 0.8 s). That means each time the program is executed, it will predict the next two complete walking steps, which is one gait period. As we mentioned before, our design of Lemma 2 requires the prediction horizon H to be chosen as the gait period or a multiple of it (that is, $H = \omega N, \omega = 1, 2, \dots$). The choice of $H = 2N$ once again strongly confirms our viewpoint in Lemma 2.

For verification, we compare the following two cases:

Case 1. The traditional DCBF, which is designed as $h_{DCBF}(v^x_{com}(k)) = \overline{V}_{DCBF} - v^x_{com}(k)$. Note that $\overline{V}_{DCBF}$ is a constant here.

Case 2. The P-DHOCBF proposed in this paper. Design $\overline{V}_{P-DHOCBF}(k)$ based on the periodicity of robot system (23), which makes $h_{P-DHOCBF}(k, v^x_{com}(k)) = \overline{V}_{P-DHOCBF}(k) - v^x_{com}(k)$ a time-periodic function.

Next, simulation results will be provided. In Fig. 4(a), it can be seen that both types of DCBFs are capable of ensuring the robot to walk steadily and guaranteeing the safety of the system. In addition, Fig. 5 illustrates a snapshot of the 12-DOF bipedal robot walking process and the periodic gait trajectories obtained via our approach. Afterwards, the angle changes of each joint over time are shown in Fig. 6.

However, as shown in Fig. 4(b), it is evident that the DCBFs in Case 1 introduce significantly greater conservatism of safety compared to the P-DHODCBFs in Case 2. To explain this more clearly, we refer to Fig. 7. First, suppose the system was initially following the reference trajectory, represented by the black line in Fig. 7. At a certain moment, an unsafe event occurs, causing the system trajectory to abruptly shift to the red line. We now discuss the two cases separately:

Case 1. Although the system deviates from the reference trajectory, it still remains within the safe zone enforced by the DCBF (the blue-shaded area in Fig. 7), meaning that the safety boundary is never actually violated. As a result, the DCBF is unable to react to this abnormal trajectory and thus cannot effectively guide it back to normal.

Case 2. The abnormal trajectory crosses the safety boundary defined by the P-DHOCBF (indicated by the yellow line). Strictly speaking, such a deviation would not occur under P-DHOCBF, which can actively intervene once the trajectory nears the safety boundary, ensuring that the trajectory remains within the safe zone (depicted as the grid-shaded area in Fig. 7).

From Fig. 4(c), it is more evident that the P-DHOCBF can prominently reduce the conservatism of safety compared to the traditional DCBF, since the smaller the value of h, the closer the system is to the safety boundary. Ignoring the initial transition phase (0 – 2 s), we calculate the average safety margin in the two cases in the subsequent periodic steady state starting from 2 s:

$$\bar{h}_{DCBF} = \frac{\sum_{k=201}^{400} h_{DCBF}(v^x_{com}(k))}{200} = 0.0226, \tag{38a}$$

$$\bar{h}_{P-DHOCBF} = \frac{\sum_{k=201}^{400} h_{P-DHOCBF}(k, v^x_{com}(k))}{200} = 0.0073. \tag{38b}$$

Therefore, the safety margin ratio of P-DHOCBF to DCBF can be calculated:

$$M = \frac{\bar{h}_{P-DHOCBF}}{\bar{h}_{DCBF}} \times 100\,\% = 32.3\,\%. \tag{39}$$

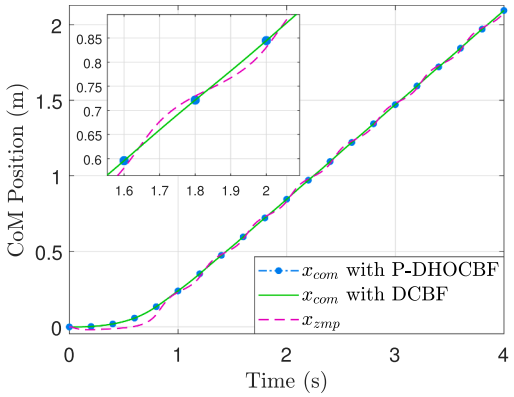

(a) CoM positions in the x-direction. There is almost no difference between the two cases.

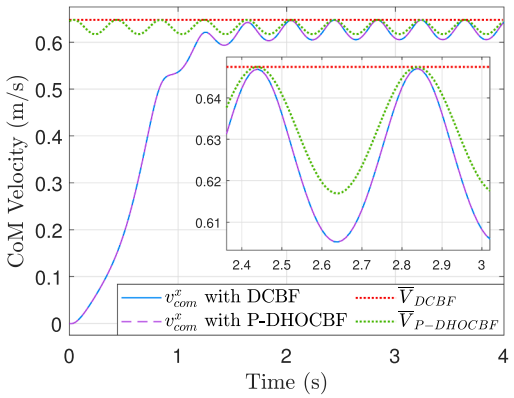

(b) CoM velocities v^x_{com} constrained by DCBF and P-DHOCBF.

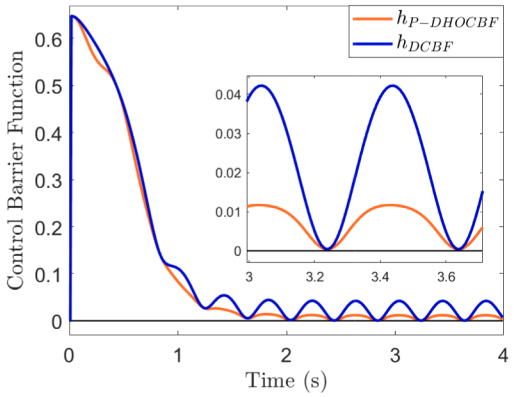

(c) Values of DCBF and P-DHOCBF. Both h functions are greater than 0, meaning that the system is guaranteed to be safe.

Fig. 4. Comparison of simulation results of the two cases.

The safety margin ratio $M = 32.3\,\% < 100\,\%$ means that P-DHOCBF reduces the conservatism in safety by about 67.7 % compared with DCBF, highlighting a key distinction between the two approaches. In other words, P-DHOCBF apparently reduces the safe zone without affecting the normal operation of the system, which can more effectively ensure safety in the event of accidents. As mentioned earlier, when unsafe events occur in the system, traditional DCBF may not be able to detect it in a timely manner, but using the P-DHOCBF can effectively avoid this situation from happening. However, it must be mentioned that while P-DHOCBF reduces the safe

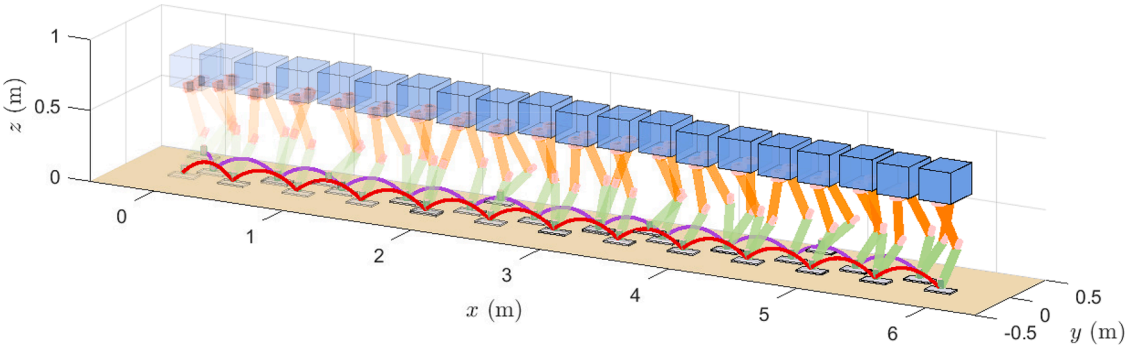

Fig. 5. Snapshots of simulation results.

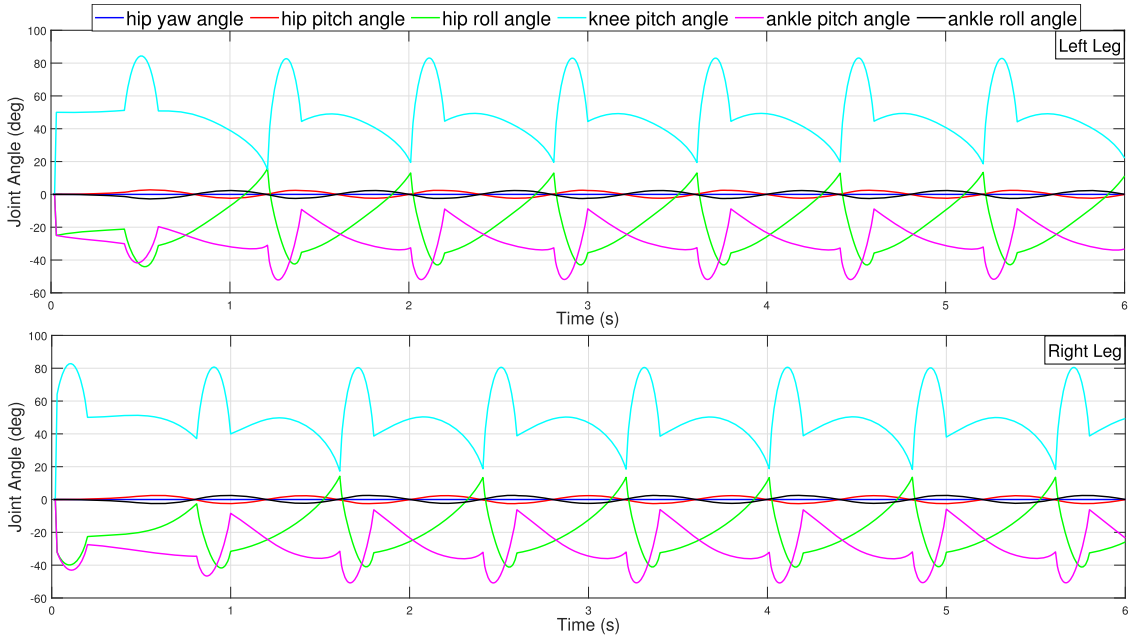

Fig. 6. Joint angles of the robot's left and right legs change over time.

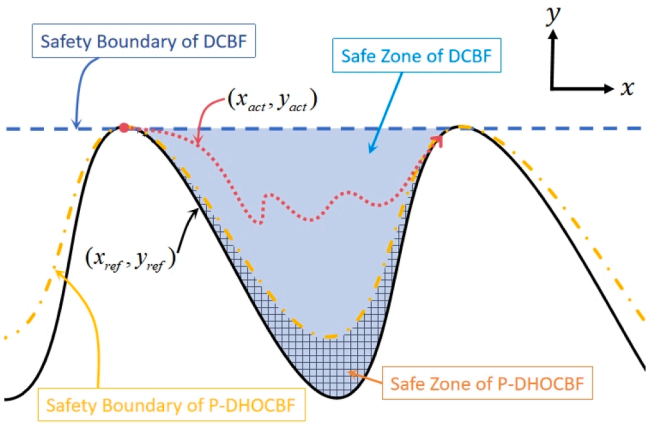

Fig. 7. Schematic diagram of unsafe situation.

zone and thereby decreases the system conservatism of safety, it may also affect the feasibility of the optimization problem. We will explore this feasibility issue in our future study.

6. Conclusion and future work

In this paper, a novel P-DHOCBF has been developed through extending DCBF to systems with periodic characteristics in system states, and it has been proven that satisfying the P-DHOCBF constraint ensures the forward invariance of the periodic safety set. Besides, the effectiveness of the proposed P-DHOCBF has been demonstrated through an illustrative example of Van der Pol oscillator. Afterwards, a P-MPC optimization problem with P-DHOCBF has been constructed. Considering the periodicity, the constraints based on P-DHOCBF of optimization problems have been formulated, and applied to the periodic forward walking of a 12-DOF bipedal robot as a simulation case study. Comparing with the existing DCBF, a quantitative analysis based on safety margin has been conducted. The results have illustrated that the conservatism of safety in systems with periodic characteristics in system states can be prominently reduced by P-DHOCBF, thereby enabling safety to be guaranteed in a timely manner.

As the primary objective of this paper is the validation of P-DHOCBF, evaluations were only conducted in relatively idealized scenarios. In practice, sensory feedback from IMU or vision-based systems often exhibits non-negligible delays and has limited sampling rates. These issues can present challenges to the overall results. Future enhancements of our proposed framework will incorporate delay-tolerant state estimators and develop robust P-MPC formulations that explicitly consider sensor delays within the prediction horizon. Besides, in future work, we will continue experiments by combining the dynamics and kinematics of actual bipedal robots, extending the application of P-DHOCBF to more complicated scenarios. Also, the impact of safe zone reduction on feasibility will also be investigated.

CRediT authorship contribution statement

Kai Zong: Writing – review & editing, Writing – original draft, Visualization, Validation, Software, Methodology, Investigation, Formal analysis, Data curation, Conceptualization; **Xiaochen Xie:** Writing – review & editing, Writing – original draft, Supervision, Resources, Project administration, Methodology, Investigation, Funding acquisition, Formal analysis, Conceptualization; **Zhaoji Ling:** Writing – review & editing, Investigation, Formal analysis; **Jing Dai:** Writing – review & editing, Methodology, Investigation; **Ka-Wai Kwok:** Writing – review & editing, Supervision, Resources, Project administration, Funding acquisition.

Declaration of competing interest

The authors declare that they have no known competing financial interests or personal relationships that could have appeared to influence the work reported in this paper.

The author is an Editorial Board Member/Editor-in-Chief/Associate Editor/Guest Editor for this journal and was not involved in the editorial review or the decision to publish this article.

Acknowledgment

This work was supported in part by National Natural Science Foundation of China under Grant 62203137, in part by Shenzhen Science and Technology Program under Grant JCYJ20250604145333044, and in part by the Research Grants Council of Hong Kong under Grants STG1/E-401/23-N, AoE/E-407/24-N, 17204124 and 17210023.

References

[1] S. Bittanti, P. Colaneri, Periodic Systems: Filtering and Control, Springer-Verlag, London, U.K., 2008.
[2] X. Xie, J. Lam, P. Li, A novel H_∞ tracking control scheme for periodic piecewise time-varying systems, Inf. Sci. 484 (2019) 71–83.
[3] P. Li, J. Lam, K.-W. Kwok, R. Lu, Stability and stabilization of periodic piecewise linear systems: a matrix polynomial approach, Automatica 94 (2018) 1–8.
[4] X. Xie, J. Lam, Guaranteed cost control of periodic piecewise linear time-delay systems, Automatica 94 (2018) 274–282.
[5] X. Xie, J. Lam, C. Fan, X. Wang, K.-W. Kwok, A polynomial blossoming approach to stabilization of periodic time-varying systems, Automatica 141 (2022) 110305.
[6] H. Muramatsu, S. Katsura, Separated periodic/aperiodic state feedback control using periodic/aperiodic separation filter based on lifting, Automatica 101 (2019) 458–466.
[7] I.M. Meza-Sánchez, L.T. Aguilar, A. Shiriaev, L. Freidovich, Y.O. and, Periodic motion planning and nonlinear H_∞ tracking control of a 3-DOF underactuated helicopter, Int. J. Syst. Sci. 42 (5) (2011) 829–838.
[8] S. Prajna, A. Jadbabaie, G.J. Pappas, A framework for worst-case and stochastic safety verification using barrier certificates, IEEE Trans. Autom. Control 52 (8) (2007) 1415–1428.
[9] P. Wieland, F. Allgöwer, Constructive safety using control barrier functions, IFAC Proc. Volumes 40 (12) (2007) 462–467.
[10] Q. Nguyen, K. Sreenath, Exponential control barrier functions for enforcing high relative-degree safety-critical constraints, in: 2016 American Control Conference (ACC), 2016, pp. 322–328.
[11] Q. Nguyen, K. Sreenath, Robust safety-critical control for dynamic robotics, IEEE Trans. Autom. Control 67 (3) (2022) 1073–1088.
[12] W. Xiao, C. Belta, High-order control barrier functions, IEEE Trans. Autom. Control 67 (7) (2022) 3655–3662.
[13] W. Shaw Cortez, D. Oetomo, C. Manzie, P. Choong, Control barrier functions for mechanical systems: theory and application to robotic grasping, IEEE Trans. Control Syst. Technol. 29 (2) (2021) 530–545.
[14] A.J. Taylor, A.D. Ames, Adaptive safety with control barrier functions, in: 2020 American Control Conference (ACC), 2020, pp. 1399–1405.
[15] M. Srinivasan, S. Coogan, Control of mobile robots using barrier functions under temporal logic specifications, IEEE Trans. Rob. 37 (2) (2021) 363–374.
[16] J. Li, Q. Nguyen, Dynamic walking of bipedal robots on uneven stepping stones via adaptive-frequency MPC, IEEE Control Syst. Lett. 7 (2023) 1279–1284.

[17] M. Leomanni, G. Bianchini, A. Garulli, R. Quartullo, Sum-of-norms periodic model predictive control for space rendezvous, IEEE Trans. Control Syst. Technol. 30 (3) (2022) 1311–1318.
[18] J. Zeng, B. Zhang, K. Sreenath, Safety-critical model predictive control with discrete-time control barrier function, in: 2021 American Control Conference (ACC), 2021, pp. 3882–3889.
[19] S. Liu, J. Zeng, K. Sreenath, C.A. Belta, Iterative convex optimization for model predictive control with discrete-time high-order control barrier functions, in: 2023 American Control Conference (ACC), 2023, pp. 3368–3375.
[20] A. Katriniok, E. Shakhesi, W.P.M.H. Heemels, Discrete-time control barrier functions for guaranteed recursive feasibility in nonlinear MPC: an application to lane merging, in: 2023 62nd IEEE Conference on Decision and Control (CDC), 2023, pp. 3776–3783.
[21] S. He, J. Zeng, K. Sreenath, Autonomous racing with multiple vehicles using a parallelized optimization with safety guarantee using control barrier functions, in: 2022 International Conference on Robotics and Automation (ICRA), 2022, pp. 3444–3451.
[22] Z. Li, J. Zeng, A. Thirugnanam, K. Sreenath, Bridging model-based safety and model-free reinforcement learning through system identification of low dimensional linear models, (2022). https://doi.org/10.48550/ARXIV.2205.05787
[23] J. Zeng, Z. Li, K. Sreenath, Enhancing feasibility and safety of nonlinear model predictive control with discrete-time control barrier functions, in: 2021 60th IEEE Conference on Decision and Control (CDC), 2021, pp. 6137–6144.
[24] J. Liu, H. Chen, P.M. Wensing, W. Zhang, Instantaneous capture input for balancing the variable height inverted pendulum, IEEE Rob. Autom. Lett. 6 (4) (2021) 7421–7428.
[25] M. Morisawa, R. Cisneros, M. Benallegue, I. Kumagai, A. Escande, F. Kanehiro, Online 3D CoM trajectory generation for multi-contact locomotion synchronizing contact, in: 2018 IEEE-RAS 18th International Conference on Humanoid Robots (Humanoids), 2018, pp. 1–8.
[26] T. Koolen, M. Posa, R. Tedrake, Balance control using center of mass height variation: limitations imposed by unilateral contact, in: 2016 IEEE-RAS 16th International Conference on Humanoid Robots (Humanoids), 2016, pp. 8–15.
[27] V.C. Paredes, A. Hereid, Resolved motion control for 3D underactuated bipedal walking using linear inverted pendulum dynamics and neural adaptation, in: 2022 IEEE/RSJ International Conference on Intelligent Robots and Systems (IROS), 2022, pp. 6761–6767.
[28] B. Li, L. Zhu, J. Huang, Stable locomotion of biped robot with gaits of sinusoidal harmonics, IEEE Trans. Control Syst. Technol. 32 (3) (2024) 805–817.
[29] Z. Li, J. Zeng, S. Chen, K. Sreenath, Autonomous navigation of underactuated bipedal robots in height-constrained environments, Int. J. Rob. Res. 42 (8) (2023) 565–585.
[30] S. Kousik, S. Vaskov, F. Bu, M. Johnson-Roberson, R. Vasudevan, Bridging the gap between safety and real-time performance in receding-horizon trajectory design for mobile robots, Int. J. Rob. Res. 39 (12) (2020) 1419–1469.
[31] B. Sangiovanni, G.P. Incremona, M. Piastra, A. Ferrara, Self-configuring robot path planning with obstacle avoidance via deep reinforcement learning, IEEE Control Syst. Lett. 5 (2) (2021) 397–402.
[32] M. Koptev, N. Figueroa, A. Billard, Real-time self-collision avoidance in joint space for humanoid robots, IEEE Rob. Autom. Lett. 6 (2) (2021) 1240–1247.
[33] M. Sun, D. Wang, Initial shift issues on discrete-time iterative learning control with system relative degree, IEEE Trans. Autom. Control 48 (1) (2003) 144–148.
[34] Y. Xiong, D.-H. Zhai, M. Tavakoli, Y. Xia, Discrete-time control barrier function: high-order case and adaptive case, IEEE Trans. Cybern. 53 (5) (2023) 3231–3239.
[35] J. Xu, B. Alrifaee, Learning-based control barrier function with provably safe guarantees: reducing conservatism with heading-aware safety margin, arXiv:2411.08999 (2024).
[36] S. Li, Z. Yuan, Y. Chen, F. Luo, Z. Yang, Q. Ye, W. Fu, Y. Fu, Optimizable control barrier functions to improve feasibility and add behavior diversity while ensuring safety, Electronics 11 (22) (2022) 3657.
[37] H.K. Khalil, Nonlinear Systems, Prentice Hall, Upper Saddle River, NJ, 2002.
[38] B. van der Pol, On oscillation hysteresis in a triode generator with two degrees of freedom, London Edinburgh Dublin Philos. Mag. J. Sci. 43 (256) (1922) 700–719.
[39] S. Kajita, H. Hirukawa, K. Harada, K. Yokoi, Introduction to Humanoid Robotics, Springer-Verlag, Berlin, 2014.
[40] S. Caron, A. Escande, L. Lanari, B. Mallein, Capturability-based pattern generation for walking with variable height, IEEE Trans. Rob. 36 (2) (2020) 517–536.
[41] T.K. Ko Yamamoto, T. Sugihara, Survey on model-based biped motion control for humanoid robots, Adv. Rob. 34 (21–22) (2020) 1353–1369.
[42] F.M. Smaldone, N. Scianca, V. Modugno, L. Lanari, G. Oriolo, ZMP constraint restriction for robust gait generation in humanoids, in: 2020 IEEE International Conference on Robotics and Automation (ICRA), 2020, pp. 8739–8745.
[43] R.C. Luo, C.C. Chen, Biped walking trajectory generator based on three-mass with angular momentum model using model predictive control, IEEE Trans. Ind. Electron. 63 (1) (2016) 268–276.
[44] F.M. Smaldone, N. Scianca, L. Lanari, G. Oriolo, From walking to running: 3D humanoid gait generation via MPC, Front. Rob. AI 9 (876613) (2022).
[45] N. Scianca, V. Modugno, L. Lanari, G. Oriolo, Gait generation via intrinsically stable MPC for a multi-mass humanoid model, in: 2017 IEEE-RAS 17th International Conference on Humanoid Robotics (Humanoids), 2017, pp. 547–552.
[46] N. Scianca, D. De Simone, L. Lanari, G. Oriolo, MPC For humanoid gait generation: stability and feasibility, IEEE Trans. Rob. 36 (4) (2020) 1171–1188.